Precision Position Measurement of Linear Motors Mover Based on Temporal Image Correlation

Jing Zhao, Jiwen Zhao, Hui Wang, Juncai Song, and Fei Dong

Abstract— **High-precision position measurement is very important for precision motion control of a linear motor. This paper presents an accurate mover position detection method with high precision stability based on temporal image correlation and fence image for the linear motors. First, sequence fence images with the information of mover position are recorded by a position measurement system for linear motor, and the integer pixel displacement of each image is obtained by image correlation method. Then, according to the continuity of the motion, the subpixel displacement can be extracted by fitting the integer pixel displacement. Finally, the displacement and velocity curves can be calculated according to system calibration. Compared to digital image measurement used in position detection of linear motors, the proposed method can detect mover position accurately with longer measurement range and smaller uncertainty. The moving least square (MLS) algorithm is used to ensure the stability of measurement uncertainty under different motion modes. Simulations and mover position detection experiments with different motion conditions were performed to demonstrate the effectiveness of the proposed method in linear motors. In this paper, the average measurement error of displacement is 0.006 mm with the maximum displacement of 120 mm. The maximum and average relative errors are less than 0.06% and 0.017%, respectively.**

Index Terms— **Linear motor, moving least square (MLS), precision position measurement, temporal image correlation.**

I. Introduction

PERMANENT-MAGNET synchronous linear motors (PMSLMs) have been widely used in many precision manufacturing devices, such as laser lithography, 3-D printer, and high-precision microcoordinate measuring machine, owing to their high speed, small thrust ripple, precision, and long working range [1]–[4]. In these applications, high motion controlling accuracy is necessary. As one of the key techniques for motion control of linear motors, accurate position detection has attracted many attentions. Especially, for some long-stroke applications, such as laser scribing of thin-film photovoltaic panels or printed circuit board drilling [5]–[7], a position detection method with high stability is also necessary. Therefore, it is of great significance to develop an accurate mover position detection method with high stability of precision for linear motors.

In the past few decades, many efforts have been made to facilitate position detection for linear motors. As the highest precise displacement measurement method, laser interferometry provides a method with nanometer resolution and uncertainty [8]. However, laser interferometer not only requires a precise alignment and assembly process but also needs a sophisticated system to avoid vibration. Linear optical encoder (namely, grating scale) is the most commonly used position sensor in linear motors [9]. Its precision depends on the grating ruling density, and the production cost is greatly increased with improved detection precision. Furthermore, thermal deformation of the grating scale may be induced by temperature disturbance [10], which will increase the position detection error. To achieve a low-cost method for position detection of linear motors, magnetic sensors such as linear Hall sensors have been studied widely [11]–[13]. However, it cannot be used in precise motion control because Hall sensor signals are contaminated by third-order harmonics, which will affect the uncertainty of position detection for linear motors. Some researchers have also adopted sensorless methods [14], [15], which can estimate mover speed and position using the voltage and current information. Sensorless methods can be grouped into many categories, of which the most representative categories are the back-electromotive force-based methods and high-frequency injection methods [16], [17]. The former is highly dependent on the uncertainty of the electrical parameter and performs poorly in low-speed conditions, whereas the latter introduces thrust ripple and extra loss. Generally, sensorless methods are inappropriate in high-precision applications.

Digital image measurement (DIM) has been successfully applied in 2-D and 3-D measurements [18]–[20], particularly for estimating displacement and strain, thanks to its advantages such as noncontact, high precision, strong robustness, and intelligence. In essence, the motion of a linear motor mover is 1-D rigid-body translation [21], [22]. The displacement vector of the mover can be obtained using DIM, which matches images captured before and after movement.

Traditional digital image measurement method, also named digital image correlation (DIC), can be divided into two stages: pixel displacement calculation and subpixel

Manuscript received June 14, 2018; revised August 29, 2018; accepted September 25, 2018. Date of publication November 2, 2018; date of current version August 9, 2019. This work was supported in part by the National Natural Science Foundation of China under Grant 51707002, Grant 51637001, and Grant 51577001 and in part by the Natural Science Foundation of Anhui Province under Grant 1808085QE123. The Associate Editor coordinating the review process was Dr. Edoardo Fiorucci. *(Corresponding author: Jiwen Zhao.)*

The authors are with the School of Electrical Engineering and Automation, Anhui University, Hefei 230601, China (e-mail: zhaojing_ustc@163.com; ustczjw@ahu.edu.cn; wanghuiahu@126.com; songjuncai528@gmail.com; feidong@ahu.edu.cn).

Color versions of one or more of the figures in this paper are available online at http://ieeexplore.ieee.org.

Digital Object Identifier 10.1109/TIM.2018.2875645

displacement calculation. The precision of the mover position detection is dependent on the precision of the subpixel displacement registrations.

To achieve precise measurement, some subpixel displacement methods have been proposed, such as the interpolation method, surface fitting method, and gradient method [23]–[26]. The interpolation method is time consuming and its uncertainty cannot meet the demands of the mover position detection. The surface fitting method utilizes a quadratic surface or Gaussian surface to fit the correlation coefficients around the pixel displacement point, and the extreme position is the subpixel displacement. This method is widely used in practical applications because of its quick speed in displacement measurement, but its antiinterference ability needs to be further improved.

To satisfy the measurement demand of strong robust for linear motors, phase correlation algorithm (PCA) is introduced in position measurement for linear motors [21], which use the frequency domain correlation to tracking mover position. Furthermore, 1-D extended PCA (EPCA) is proposed to reduce the uncertainty of subpixel displacement and improve calculation efficiency [22].

The method in [22] exhibits high precision and stability in small measurement range but fails in larger displacement, because its uncertainty is greatly related to measurement range. For example, the measurement error will increase sharply when the displacement exceeds 16 pixels approximately for an image with the size of 64×256 pixels. Enlarging images size is a means to increase measurement range, but large images involve a considerable amount of data and reduce the real-time performance for linear motors. Therefore, it is necessary to develop a subpixel displacement extraction algorithm with a longer measurement range for position estimation of linear motors.

Another question is that the motion of the linear motor is usually not a monotonous mode; therefore, the position detection method should be robust in different working conditions. To monitor mover position with long measurement range and different motion modes, a precise and dynamic measurement method named temporal image correlation method is applied. The method takes into account the continuity of the mover displacement along the time axis instead of just spatial correlation. A mover position detection system is established with a fence image as the capturing target and sequence of images are recorded by a high-speed camera. The pixel displacement of each image is retrieved *in situ* using single-line sampling and a correlation matching algorithm. To guarantee the measurement stability under different motion modes, moving least square (MLS) fitting algorithm is used to fit the pixel displacement curve along the time axis, and then the precise displacement of the mover can be obtained.

The advantages of the temporal image correlation for mover position detection are summarized as follows.

1) Compared to the traditional DIC and EPCA methods, it can monitor mover position accurately with longer measurement range and smaller uncertainty under different motion modes.

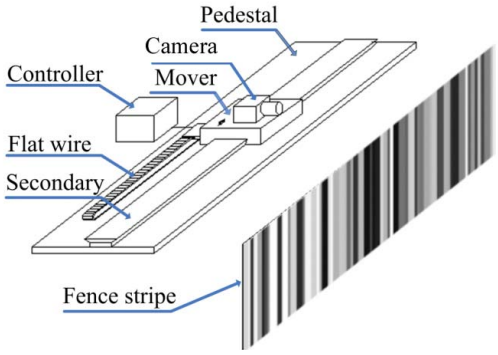

Fig. 1. Schematic of the mover position detection system.

2) The fence image is designed as a target image, and single-line sampling algorithm is applied to keep the computation complexity as low as possible, in order to permit the real-time application of this technique.

The rest of this paper is organized as follows. Section II describes the principle of the method in detail. Section III studies its stability and measurement uncertainty with different motion modes by simulation. The subpixel displacement extraction algorithms based on least squares (LSs) and MLSs) are compared and their application conditions are also discussed. In Section IV, a position detection platform for the linear motor is performed and the availability of the proposed method in linear motor mover position estimation is verified. Finally, the conclusion is given in Section V.

II. Principle of the Mover Position Detection Based on the Temporal Image Correlation Method

The schematic of the mover position detection system with a fence image is shown in Fig. 1. Due to the only horizontal 1-D movement of the linear motor, the target image prepared for image correlation algorithm is designed as a fence image to suppress the influence of longitudinal vibration and reduce the computational complexity [21], [22]. The fence stripe image can be defined as

$$W_x = \max\left(\sum_{y=1}^{M_0}\sum_{x=2}^{N_0}|G_x|\right) \tag{1}$$

$$W_y = \sum_{y=1}^{M_0}\sum_{x=2}^{N_0}|G_y| = 0 \tag{2}$$

where G_x, G_y, W_x, and W_y are the intensity gradient and the gradient sum of the horizontal and vertical directions, respectively. The size of the image is $M_0 \times N_0$ pixels.

To avoid the image matching error caused by the periodicity of fence images, a more robust fence image with nonperiodicity is selected as the target image and its robustness is discussed in detail in [27]. The fence image is printed on a plane perpendicular to the pedestal of the linear motor, and a camera is installed on the mover. When the motor is moving, fence image sequences, which contain mover displacement information, are captured successively by setting the capturing interval.

To detect the mover position of linear motors precisely, temporal image correlation method is proposed to retrieve the displacement curve from the sequence of fence images. The proposed method can be divided into two stages: pixel displacement stage and subpixel displacement stage. First, the single-line sampling algorithm is used to reduce data complexity and improve efficiency. Then, a correlation matching algorithm is utilized to obtain integer pixel displacement of each image in real time. Finally, according to the continuity of the displacements in time, an LS or MLS fitting algorithm is used to fit the pixel displacement curve and obtain the subpixel displacement.

A. Pixel Displacement Calculation Based on Correlation Matching Algorithm

With the movement of the linear motor, the sequence of images $It(x, y)$ can be recorded by the charge-coupled device (CCD) camera. Subsequently, the pixel displacement can be retrieved by a correlation matching algorithm.

In this process, the selection of shape function is important, because it is strongly related to the traditional DIC implement, in particular for complex deformations [28], [29]. Shape functions are used to describe the displacement relationship between the current image and the reference image. For linear motors, the motion of a mover is 1-D rigid-body translation along the x-axis in essence. Hence, zero-order shape function is selected in this paper, which is expressed as

$$\begin{cases} x = x_0 + u \\ y = y_0 \end{cases} \tag{3}$$

where (x, y) and (x_0, y_0) denote the point of the current image and reference image, respectively. $[u, 0]$ are displacement parameters.

Therefore, the relationship between the current image and the reference image can be expressed, mathematically, as

$$I_t(x, y) = I_0(x_0 + u(t), y_0), \quad t = 0, \Delta t, 2\Delta t \cdots N\Delta t \tag{4}$$

where N and Δt are the frame number and captured interval, respectively. The reference image $I_0(x_0, y_0)$ denotes the image captured by the camera at time $t = 0$, and $u(t)$ is the displacement of the mover to be detected.

Subsequently, a single-line sampling algorithm is applied and the 2-D image can be transformed into a 1-D gray curve. Equation (1) is simplified as

$$f_t(x) = f_0(x_0 + u(t)) \tag{5}$$

where $f_t(x)$ and $f_0(x_0)$ denote the stripe signals retrieved from the current image and the reference image, respectively.

The current signal is then compared with the reference signal using a predefined correlation function to describe the difference of two signals. A typical correlation function (named zero-mean normalized cross correlation function [30]) is selected, which is insensitive to light. It can be defined as

$$C(u^*(t)) = \frac{\sum_{-m}^{m} [f_t(x) - \overline{f_t}] \times [f_0(x_0) - \overline{f_0}]}{\sqrt{\sum_{-m}^{m} [f_t(x) - \overline{f_t}]^2} \times \sqrt{\sum_{-m}^{m} [f_0(x_0) - \overline{f_0}]^2}} \tag{6}$$

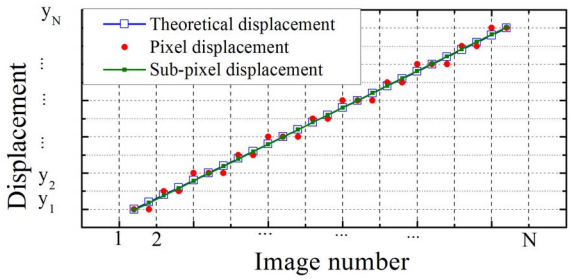

Fig. 2. Principle diagram of subpixel displacement extraction.

where $\overline{f_t}$ and $\overline{f_0}$ denote the average gray value of the current signal and the reference signal, respectively. m is the length of the signal. $C(u^*(t))$ is the correlation coefficient matrix. $u^*(t)$ is the displacement evolution.

However, the displacement $u^*(t)$ calculated by (6) is an integral multiple of one pixel dimension due to the discrete aspect of digital images. Subpixel algorithms are required to further reduce the measurement uncertainty.

It is worth noting that, for the traditional DIC, the selection of correlation function is directly related to the calculation efficiency and uncertainty of the subpixel displacement, especially for noisy images [28], [29]. Since the temporal image correlation method uses the temporal continuity of the displacement instead of the spatial correlation coefficient matrix to obtain the subpixel displacement, the correlation function type and noise have little effect on the measurement uncertainty.

B. Subpixel Displacement Extraction Based on MLS Algorithm

The commonly used subpixel solving methods are based on the spatial information iteration of pixel points. However, when the displacement is large, the iteration method is too time-consuming. Because the mover motion is continuous and regular, the subpixel displacement can be obtained by the law of mover motion on the time axis. The principle of the method can be summarized that the subpixel displacement is obtained by fitting the pixel displacement evolution, as shown in Fig. 2. The principle diagram suggests that the uncertainty of subpixel displacement is directly related to image number and fitting method. In this paper, LS and MLS fitting methods are used to extract the subpixel displacement.

In the MLS method, the subpixel approximated function in a subdomain (influence domain) of the fitting region can be written as

$$f(x) = \mathbf{p}(\mathbf{x})^T \mathbf{a}(\mathbf{x}) = \sum_{j=0}^{n} a_j(x) x^j \tag{7}$$

where x is the image number in the influence domain, $\mathbf{p(x)} = [1, x, \cdots x^n]^T$ is the basis function vector, and $\mathbf{a(x)} = [a_0(x), a_1(x), \cdots a_n(x)]^T$ is the undetermined coefficient, which is dependent on the x coordinate.

The undetermined coefficient $\mathbf{a(x)}$ can be solved by minimizing the error between the pixel displacement and its approximation at tcche sampling points. The error $\mathbf{E(x)}$ is

defined as

$$\mathbf{E(x)} = \sum_{i=1}^{N} w(x - x_i)(f(x_i) - y_i)^2 = \sum_{i=1}^{N} w(x - x_i)(a_0 + a_1 x + \cdots a_n x^n - y_i)^2 \quad (8)$$

where N is the number of samples in the influence domain; $w(x - x_i)$ is the weight function, whose value is dependent on the distance between x and the sampling point x_i; and y_i is the pixel displacement at the sampling point x_i.

Solving partial derivative equation $\partial \boldsymbol{E}/\partial a = 0$, the minimum error $\mathbf{E(x)}$ and the unknown coefficient $\mathbf{a(x)}$ can be obtained

$$\frac{\partial \mathbf{E}}{\partial \mathbf{a_j}} = 2\sum_{i=1}^{N} w(x - x_i) x_i^j (a_0 + a_1 x_i + \cdots + a_n x_i^n - y_i) = 0$$

$$\cdot \begin{bmatrix} \sum_{i=1}^{N} w(x-x_i) & \sum_{i=1}^{N} w(x-x_i)x_i & \cdots \sum_{i=1}^{N} w(x-x_i)x_i^n \\ \sum_{i=1}^{N} w(x-x_i)x_i & \sum_{i=1}^{N} w(x-x_i)x_i^2 & \cdots \sum_{i=1}^{N} w(x-x_i)x_i^{n+1} \\ \sum_{i=1}^{N} w(x-x_i)x_i^n & \sum_{i=1}^{N} w(x-x_i)x_i^{n+1} & \cdots \sum_{i=1}^{N} w(x-x_i)x_i^{2n} \end{bmatrix} \cdot \begin{bmatrix} a_0 \\ a_1 \\ \vdots \\ a_n \end{bmatrix} = \begin{bmatrix} \sum_{i=1}^{N} w(x - x_i) y_i \\ \sum_{i=1}^{N} w(x - x_i) x_i y_i \\ \sum_{i=1}^{N} w(x - x_i) x_i^n y_i \end{bmatrix}. \quad (9)$$

If the left coefficient matrix of the equation is defined as $\boldsymbol{A}$, and the right coefficient matrix is written as $\boldsymbol{B}$, (9) can be rewritten in matrix form as

$$\mathbf{Aa(x)} = \mathbf{B}. \quad (10)$$

When $|\mathbf{A}| \neq 0$, the unknown coefficient $\mathbf{a(x)}$ can be obtained from the following:

$$\mathbf{a(x)} = \mathbf{A^{-1}B}. \quad (11)$$

The uncertainty of MLS is also dependent on the weight function. In MLS, the weight function must exhibit compact-supported feature, that is, a heavy weight is imposed to the points closer to the prediction point and a lightweight for more distant points. Besides, there other conditions must be satisfied: nonnegative, monotone decreasing, and smoothness. There are many weight functions that satisfy the above conditions, such as Gaussian, exponential, spline, and radial basis function [31], [32]. Among them, the spline function is one of the most commonly used weight function.

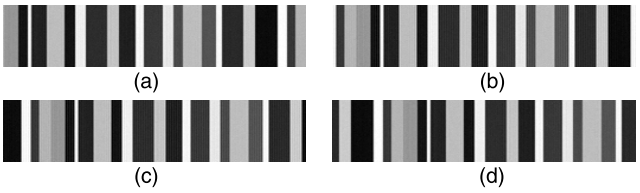

Fig. 3. Sequence of fringe patterns. (a) Initial fence image. (b) Fence image with displacement of 20.064 pixels. (c) Fence image with displacement of 40.128 pixels. (b) Fence image with displacement of 60 pixels.

Therefore, in this paper, cubic spline function is employed as the weight function, which can be expressed as

$$w(r) = \begin{cases} \frac{2}{3} - 4r^2 + 4r^3 & r \leq 1/2 \\ \frac{4}{3} - 4r^2 + 4r^3 - \frac{4}{3}r^3 & 1/2 < r \leq 1 \\ 0 \end{cases} \quad (12)$$

where $r = |x - x_i| / D_{mi}$ is the normalized distance and D_{mi} is the size of the influence domain, which directly influence fitting efficiency and accuracy. To avoid singularity, the value of D_{mi} should be large enough to guarantee sufficient sampling points within the domain. However, a too large value will result in the neglect of local features and increase in computation. In this paper, the basis function is two order polynomials, and the influence domain size is 16 pixels.

III. Simulation Experiments and Results Analysis

To verify the advantages of the mover position detection method in measurement uncertainty and measurement stability, several simulation experiments under different motion modes were carried out. All the codes are compiled by MATLAB R2008b and the computer configuration parameters used in the simulation are as follows: CPU, Intel(R) Core(TM) i5-3470; computer main frequency, 3.20 GHz; and RAM, 3.47 GB.

A. Measurement Stability Analysis

To facilitate the accurate long-stroke tracking for linear motors, the stability of the position measurement method should be analyzed. According to (3) and (4), a fence image with the size of 64 × 256 pixels is simulated, as shown in Fig. 3(a). Considering the influence of noise, Gaussian noise (0, 0.0007) is added into Fig. 3(a). Fourier transform is used to translate the target image with different displacements [33], which can be expressed mathematically, as, $I_t(x - u(t), y) \Leftrightarrow F(\xi, \eta)e^{-j2\pi[u(t)\xi]}$, where $F(\xi, \eta)$ is the Fourier transform of the reference image.

Then, a sequence of fringe patterns of uniform motion captured by the mover position detection system can be simulated. Fig. 3(b)–(d) shows images with displacements of 20.064, 40.128, and 60 pixels relative to Fig. 3(a).

In general, the maximum measurement range is related to the size of the image. To avoid mismatching in the pixel displacement stage, the maximum displacement should be less than half of the image size. In this paper, the maximum simulated displacement is 60 pixels, and the displacement can be translated into mover position according to the

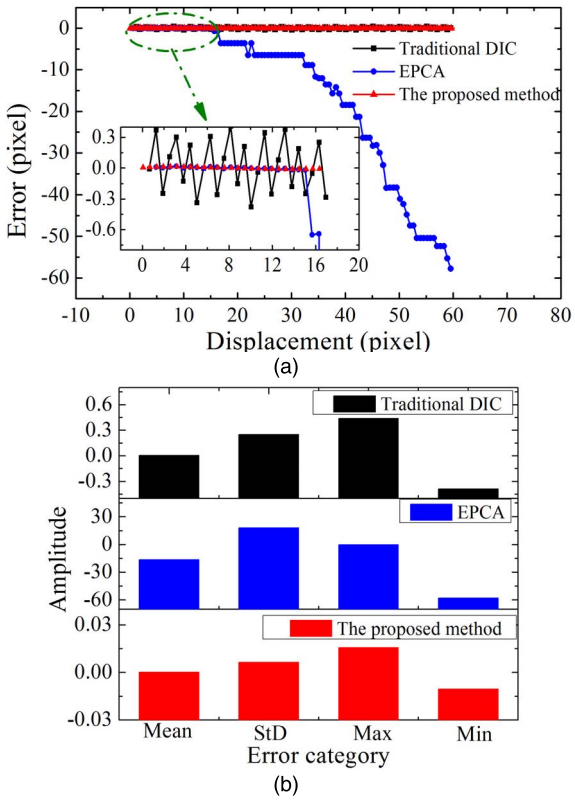

Fig. 4. Stability analysis. (a) Error curves of the traditional DIC, EPCA, and the proposed method. (b) Error statistical analysis.

system magnification. For convenience, in the following simulation experiments, the units of displacements are pixels.

Fig. 4(a) shows the error curves of displacement obtained by the traditional DIC, EPCA, and the proposed method. From the overall trend, all error curves change little when the displacement is less than 15 pixels. However, the measurement uncertainty of EPCA increases sharply with the increase in displacement. It indicates that the traditional DIC and the proposed method exhibit higher measurement stability than EPCA.

The errors curves are then zoomed to reveal more details of the uncertainty of the three methods. The maximum errors of the traditional DIC, EPCA, and the proposed method are 0.4, 0.017, and 0.016 pixels, respectively. It suggests that the uncertainty of the proposed method is much smaller than that of the traditional DIC.

To further clarify the stability of the proposed method, the error statistics histograms are shown in Fig. 4(b). The maximum error, mean error, and the standard deviation of the proposed method are 0.015, 0.002, and 0.007 pixels, respectively, which are better than the error distributions of the traditional DIC method and EPCA. Therefore, it is demonstrated that the temporal image correlation method can achieve accurate displacement detection with higher measurement stability.

B. Measurement Uncertainty Analysis With Different Fitting Methods Under Different Motion Modes

Three experiments were conducted to simulate the uniform motion, accelerated motion, and reciprocating motion of a linear motor, and the simulated displacement curves are

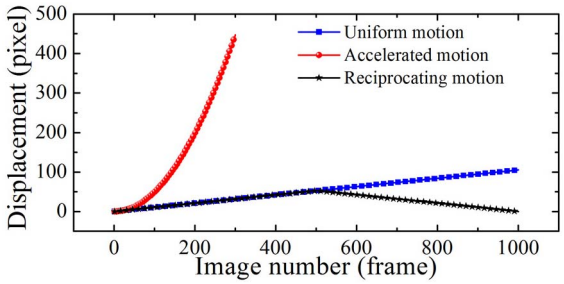

Fig. 5. Different motion modes of the linear motor.

shown in Fig. 5. The displacement of uniform motion was $s = 0.1053 \times N$ with the maximum displacement of 105.2 pixels, where N is the image number. For accelerated motion, the displacement was simulated as $s = 0.005 \times N^2$ with the maximum displacement of 447.005 pixels, and for reciprocating uniform motion, the velocity was set to ± 0.1053 pixel/frame. The initial image is 139×1344 pixels. According to the above-mentioned formulas, sequences of images with corresponding displacements can be generated using Fourier transform. Subsequently, the mover position can be detected using the proposed method. In contrast, the LS algorithm was also used to reconstruct the continuous displacement curve.

The error curves of displacement and velocity for the uniform motion are shown in Fig. 6, which are calculated by the proposed method with MLS and LS algorithms. The comparison of the error curves shows that the uncertainty is nearly the same and the maximum absolute error is about 0.026 pixels. Therefore, under uniform motion, both subpixel displacement extraction algorithms can achieve precise detection.

Figs. 7 and 8 show the results of the accelerated motion and reciprocating motion. As shown in Figs. 7(a) and 8(a), the positioning errors of accelerated motion and reciprocating motion obtained by MLS are 0.013 and 0.025 pixels, while the results of LS are 0.006 and 3.213 pixels. The velocity uncertainty of LS is better than that of MLS in accelerated motion, but for reciprocating motion, the average velocity error of MLS is lower than that of LS. It manifests that both subpixel fitting methods can provide precise measurement in displacement and velocity retrieval. LS is suitable for monotonic movement, while MLS shows more superiority over LS under reciprocating motion. In practical motor motion control or mover positioning, the single mode of movement occurs rarely. Therefore, to facilitate complex movements and ensure its positioning uncertainty, the MLS is recommended in the next experiments of the linear motor.

From the above three kinds of experiments, we can see that the temporal image correlation can provide a solution for the precise position detection of the linear motor. Especially, the subpixel algorithm with MSL fitting can ensure the stability of measurement uncertainty under different motion modes.

C. Measurement Uncertainty Analysis With Different Image Numbers

As discussed in the principle of the proposed method, the uncertainty is also determined by image number except for

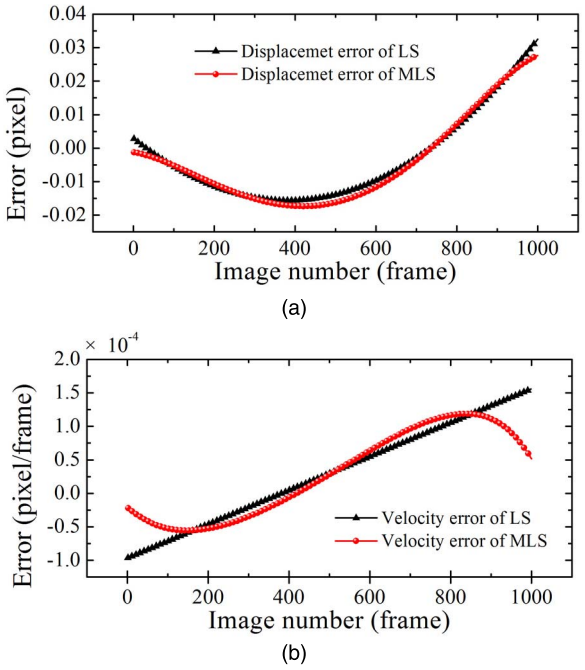

Fig. 6. Results of uniform motion. (a) Displacement error curves obtained by MLS and LS. (b) Velocity error curves obtained by MLS and LS.

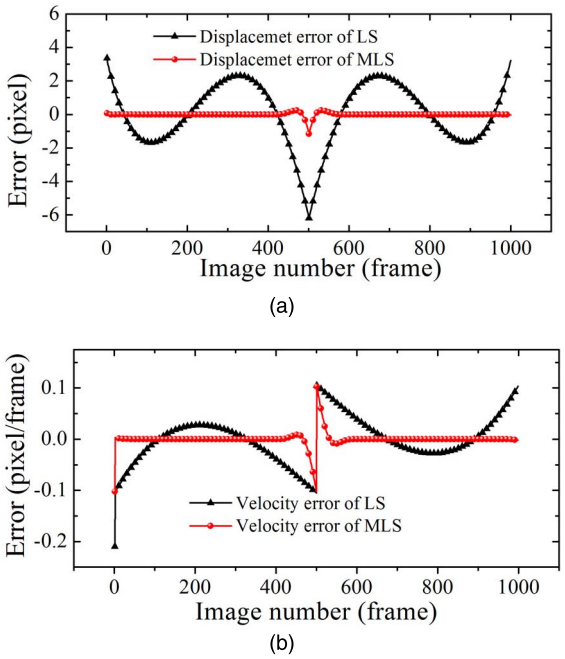

Fig. 8. Results of reciprocating motion. (a) Displacement error curves obtained by MLS and LS. (b) Velocity error curves obtained by MLS and LS.

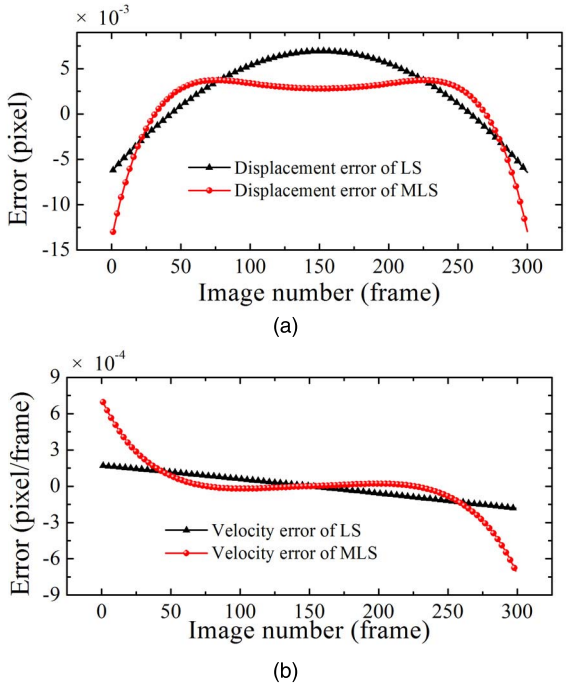

Fig. 7. Results of accelerated motion. (a) Displacement error curves obtained by MLS and LS. (b) Velocity error curves obtained by MLS and LS.

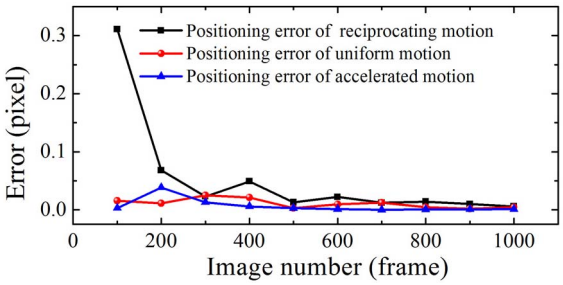

Fig. 9. Positioning error with different image numbers.

fitting method. To investigate the influence of image number on the uncertainty of the method, uniform, accelerated, and reciprocating motions experiments with different image numbers were conducted, respectively. The displacements were all constructed by MLS algorithm, and the positioning error was shown in Fig. 9. Positioning detection error for uniform motion and acceleration motion fluctuates around 0.03 pixels. However, the positioning error of reciprocating motion is greatly affected by the number of images. When the image number is 100 frames, the error exceeds 0.3 pixels. With the increase in image number, the error gradually decreases and approaches 0.03 pixels, but the improvement in uncertainty is not significant when the number of images exceeds 500 frames. To reduce the uncertainty of position detection for linear motors, more images should be involved in the subpixel algorithm. However, to too many images may lead to much time delay. Therefore, the rapidness of the proposed method should be discussed to balance the calculation time and detection uncertainty.

D. Real-Time Performance Analysis

To verify the rapidness of the algorithm in contrast with the other digital image measurement algorithm, the time delay of the traditional DIC, EPCA, and the proposed method is listed in Table I. Moreover, the influence of the image number on the time delay of the proposed method is also discussed.

A total of 800 images with 139 × 1344 pixels resolution were involved in the calculation. The pixel calculation time of these methods was the same (0.001 s/frame). The average times consumed by subpixel fitting were 0.631, 0.003, 0.001,

TABLE I
REAL-TIME PERFORMANCE COMPARISON BETWEEN TRADITIONAL DIC, EPCA, AND TEMPORAL IMAGE CORRELATION METHOD

Parameter	Traditional DIC	EPCA	Temporal image correlation
Image size (pixel)	139×1344	139×1344	139×1344
Image number (frame)	800	800	800
Time of the pixel correlation (s/frame)	0.001	0.001	0.001
Average time delay of sub-pixel calculation (s/frame)	0.631	0.003	0.001 (LS) 0.007 (MLS)

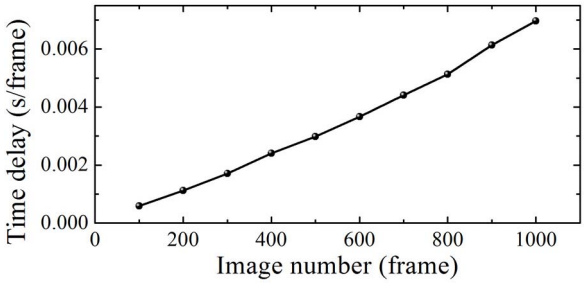

Fig. 10. Time delay with different image numbers.

and 0.007 s/frame for traditional DIC, EPCA, LS, and MLS algorithms, respectively. The comparison suggests that the subpixel algorithm takes up more than 95% of the total time for the traditional DIC. Much less time is consumed by EPCA and temporal image correlation, and the computing efficiency has been increased by nearly 90× compared to the traditional DIC. Therefore, it can be concluded that the temporal image correlation method can estimate the displacement rapidly. Although the calculation efficiency of EPCA is the fastest, the temporal image correlation method shows more advantages in long-distance measurements.

The time delay with different image numbers of the proposed method is also analyzed, as shown in Fig. 10. The consumed time is proportional to the image number. To improve the response speed, the image number should be smaller, which is in contradiction with the conclusion that more images should be used to reduce the detection uncertainty. Therefore, a balance should be sought between image number and detection uncertainty. In this paper, the image number from 300 frames to 500 frames is recommended. In the further researches, some attempts such as GPU programing or parallel computing [34] can also be employed to further improve the processing speed.

IV. EXPERIMENTAL VALIDATION AND RESULTS ANALYSIS

Two practical experiments are conducted to further confirm the feasibility and reliability of the proposed method for linear motors. According to the schematic of the mover position detection system as shown in Fig. 1, a position detection platform for the linear motor is established, as shown in Fig. 11. The motor used in this platform is a PMSLM with an effective stroke of 380 mm. The motor is driven by

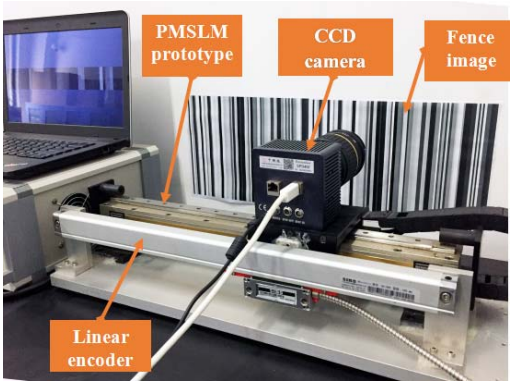

Fig. 11. Mover position detection platform of the linear motor.

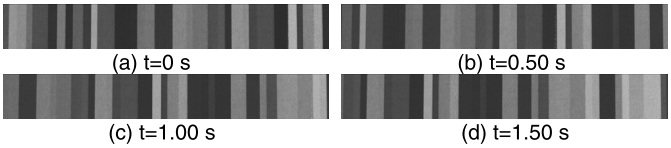

Fig. 12. Sequence of fence images captured by camera. (a) $t = 0$ s. (b) $t = 0.50$ s. (c) $t = 1.00$ s. (d) $t = 1.50$ s.

a TMS320F2812 DSP system based on the PI control strategy. A linear incremental encoder with a stroke of 300 mm and an effective resolution of 5 μm is installed as a position feedback sensor for comparison.

In practical applications, the motion blur effect cannot be ignored, because it can lead to a significant increase of uncertainty [18]. For linear motors, the motion blur effect is mainly related to the long exposure time of the camera, especially under high-speed working conditions.

In this paper, to eliminate the effect of motion blur on measurement results as much as possible, a high-speed camera is employed. The CCD camera with the pixel size of 7×7 μm is produced by Revealer of China, and the captured interval is set to 4 ms. The maximum view field of the camera is 2320 × 240 pixels. Magnification has been calibrated, and one pixel denotes 0.09974 mm in this paper. To ensure the measurement uncertainty under complex movement modes, the MLS fitting method is employed in practical experiments.

The first experiment was conducted with a piecewise motion. The motor run at a uniform speed of 0.05 m/s, and then stopped after 2.0 s. The total running time and the maximum displacement are 4.0 s and 102.545 mm, respectively. The sequence of fence images recorded by the platform is shown in Fig. 12. It indicates that there is a relative rigid-body movement perpendicular to the stripe direction between each picture. Subsequently, a temporal image correlation is implemented to extract the displacement and velocity curves from the recorded image sequence.

The measurement results of piecewise motion obtained by the proposed method and the linear encoder are compared in Fig. 13. Both the displacement and velocity obtained by the proposed method are in good agreement with the results of the linear encoder. To further clarify the detection uncertainty of this method, the error curves were analyzed, as plotted in Fig. 13(b) and (d). During uniform move-

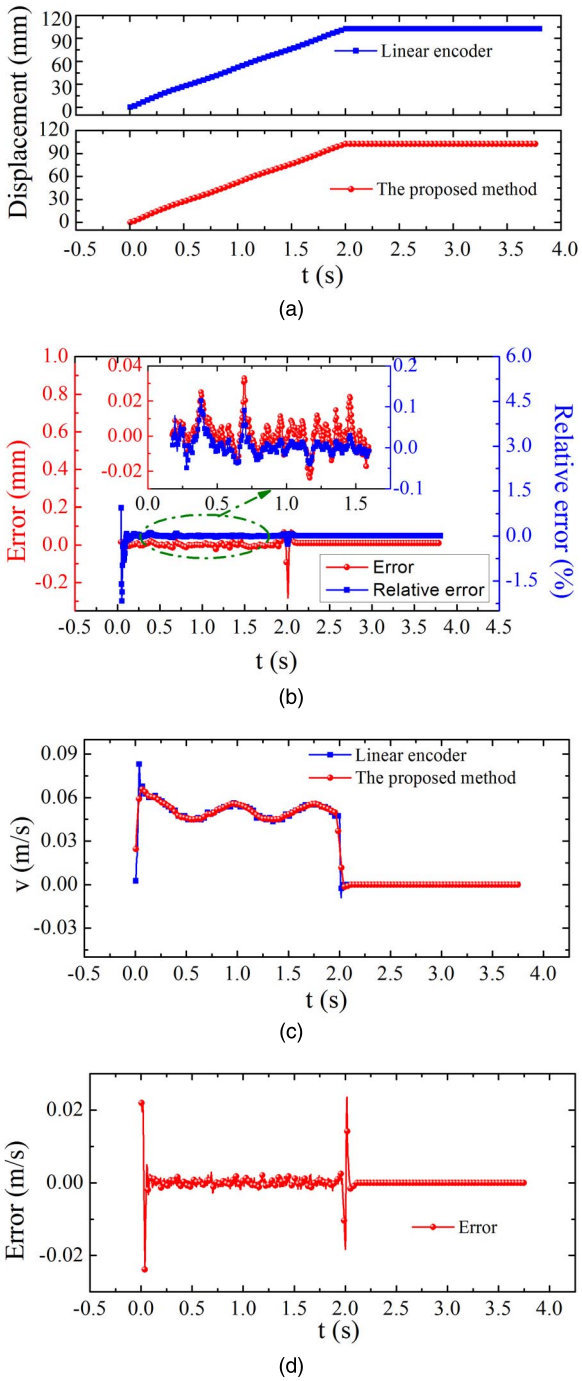

Fig. 13. Results of piecewise motion. (a) Displacement curves. (b) Displacement error curves. (c) Velocity curves. (d) Velocity error curve.

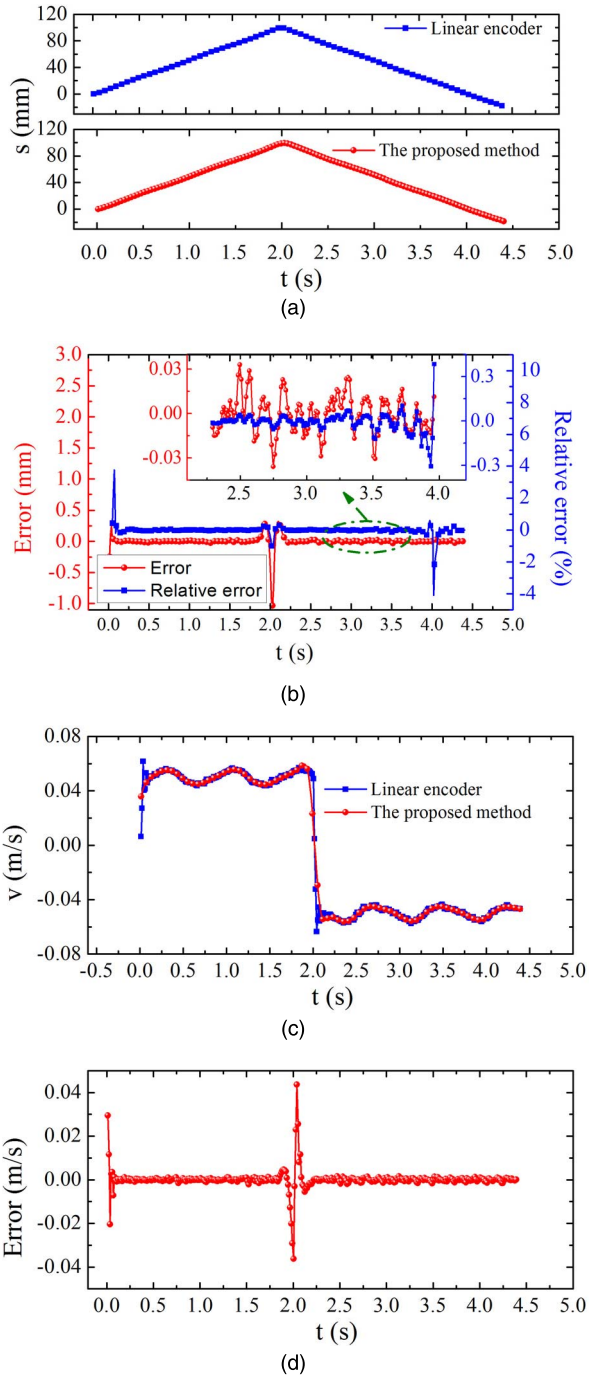

Fig. 14. Results of reciprocating motion. (a) Displacement curves. (b) Displacement error curves. (c) Velocity curves. (d) Velocity error curve.

ment stage, the maximum error and relative error of displacement are 0.035 mm and 0.06%. The average error and relative error are 0.006 mm and 0.017%. The positioning detection error is 0.010 mm during the stop stage. The average velocity is 0.0512 m/s, and the velocity error fluctuates from −0.003 to 0.003 m/s, irrespective of start and stop stages. The relative velocity error is less than 6%. It demonstrates that the proposed method can obtain the position and velocity precisely under the piecewise motion for the linear motor. The error is larger at the start and stop points for both displacement and velocity curves. This is because the image number is not sufficient to fit the accurate displacement at the turning points. We believe that the error can be further reduced by increasing image acquisition frequency at these points.

To check the availability of the temporal image correlation in more complex motion, an experiment of reciprocating motion for PMSLM is carried out at a speed of ±0.05 m/s. The total running time is 4.5 s. The mover position and velocity are retrieved by the proposed method, and the comparison results with the linear encoder are shown in Fig. 14. The phenomena

are basically the same as the first experiment. Removing the starting point and turning point, the absolute error of the displacement and velocity is less than 0.035 mm and 0.002 m/s, respectively. The relative error at $t = 4$ s is larger, because the detection error is changeless but the displacement becomes to zero. Therefore, the precision stability of temporal image correlation method is proved and can be used in precise mover position detection with different motion conditions.

V. Conclusion

This paper presents a precise mover position detection measurement method based on temporal image correlation and fence image. The accurate mover displacement, that is, subpixel displacement in DIM, can be obtained by fitting the pixel displacement directly according to the continuity of the motion. Its measurement range and uncertainty are analyzed. Compared with digital image methods in position tracking for the linear motor, the method has advantages in measurement range and stability. Different fitting algorithms are discussed and MLS algorithm is recommended achieving precise measurement in complex movement modes. The time delay is compared with the conventional DIC method, the computational efficiency of temporal image correlation increases by nearly 90×, and an appropriate amount of images is given to balance the efficiency and measurement uncertainty. A position detection platform for linear motors is also established to validate the feasibility of the method. The maximum and average errors of the position detection motion are 0.035 and 0.006 mm, respectively. The velocity error is less than 0.003 m/s. If used as a commercial application, the detection error can be further reduced by increasing the system magnification, and a faster programing mode can be employed to achieve the real-time response.

References

[1] I. Boldea, L. N. Tutelea, W. Xu, and M. Pucci, "Linear electric machines, drives, and MAGLEVs: An overview," *IEEE Trans. Ind. Electron.*, vol. 65, no. 9, pp. 7504–7515, Sep. 2018.

[2] K.-S. Low and M.-T. Keck, "Advanced precision linear stage for industrial automation applications," *IEEE Trans. Instrum. Meas.*, vol. 52, no. 3, pp. 785–789, Jun. 2003.

[3] L. Qiu, Y. Shi, J. Pan, and B. Zhang, "Robust cooperative positioning control of composite nested linear switched reluctance machines with network-induced time delays," *IEEE Trans. Ind. Electron.*, vol. 65, no. 9, pp. 7447–7457, Sep. 2018.

[4] S. Du, J. Hu, Y. Zhu, and M. Zhang, "An improved displacement measurement based on model reconstruction for permanent magnet synchronous motor," *IEEE Trans. Instrum. Meas.*, vol. 66, no. 11, pp. 3044–3051, Nov. 2017.

[5] P.-Y. Chen, W.-Y. Jywe, M-S. Wang, and C.-H. Wu, "Application of blue laser direct-writing equipment for manufacturing of periodic and aperiodic nanostructure patterns," *Precis. Eng.*, vol. 46, pp. 263–269, Oct. 2016.

[6] J. F. Pan, N. C. Cheung, and Y. Zou, "Design and analysis of a novel transverse-flux tubular linear machine with gear-shaped teeth structure," *IEEE Trans. Magn.*, vol. 48, no. 11, pp. 3339–3343, Nov. 2012.

[7] H. Butler, "Adaptive feedforward for a wafer stage in a lithographic tool," *IEEE Trans. Control Syst. Technol.*, vol. 21, no. 3, pp. 875–881, May 2013.

[8] R. Paris, M. Melik-Merkumians, and G. Schitter, "Probabilistic absolute position sensor based on objective laser speckles," *IEEE Trans. Instrum. Meas.*, vol. 65, no. 5, pp. 1188–1196, May 2016.

[9] R. Cao, M. Cheng, and B. Zhang, "Speed control of complementary and modular linear flux-switching permanent-magnet motor," *IEEE Trans. Ind. Electron.*, vol. 62, no. 7, pp. 4056–4064, Jul. 2015.

[10] W. Feng, Z. Li, Q. Gu, and J. Yang, "Thermally induced positioning error modelling and compensation based on thermal characteristic analysis," *Int. J. Mach. Tools Manuf.*, vol. 93, no. 6, pp. 26–36, Jun. 2015.

[11] J. Kim, S. Choi, K. Cho, and K. Nam, "Position estimation using linear Hall sensors for permanent magnet linear motor systems," *IEEE Trans. Ind. Electron.*, vol. 63, no. 12, pp. 7644–7652, Dec. 2016.

[12] X. Song, J. Fang, and B. Han, "High-precision rotor position detection for high-speed surface PMSM drive based on linear Hall-effect sensors," *IEEE Trans. Power Electron.*, vol. 31, no. 7, pp. 4720–4731, Jul. 2016.

[13] Y.-P. Yang and Y.-Y. Ting, "Improved angular displacement estimation based on Hall-effect sensors for driving a brushless permanent-magnet motor," *IEEE Trans. Ind. Electron.*, vol. 61, no. 1, pp. 504–511, Jan. 2014.

[14] J. Cai and Z. Deng, "Initial rotor position estimation and sensorless control of SRM based on coordinate transformation," *IEEE Trans. Instrum. Meas.*, vol. 64, no. 4, pp. 1004–1018, Apr. 2014.

[15] J. F. Pan, N. Cheung, and G. Cao, "The direct-drive sensorless generation system for wave energy utilization," *Int. J. Elect. Power Energy Syst.*, vol. 62, no. 3, pp. 29–37, Nov. 2014.

[16] W. Zhao, M. Cheng, K. T. Chau, R. Cao, and J. Ji, "Remedial injected-harmonic-current operation of redundant flux-switching permanent-magnet motor drives," *IEEE Trans. Ind. Electron.*, vol. 60, no. 1, pp. 151–159, Jan. 2013.

[17] G. Foo and M. F. Rahman, "Sensorless direct torque and flux-controlled IPM synchronous motor drive at very low speed without signal injection," *IEEE Trans. Ind. Electron.*, vol. 57, no. 1, pp. 395–403, Jan. 2010.

[18] A. Lavatelli and E. Zappa, "A displacement uncertainty model for 2-D DIC measurement under motion blur conditions," *IEEE Trans. Instrum. Meas.*, vol. 66, no. 3, pp. 451–459, Mar. 2017.

[19] M. Kinsner, D. Capson, and A. Spence, "Accurate measurement of surface grid intersections from close-range video sequences," *IEEE Trans. Instrum. Meas.*, vol. 61, no. 4, pp. 1019–1028, Apr. 2012.

[20] X. Li, W. Xu, M. A. Sutton, and M. Mello, "In situ nanoscale in-plane deformation studies of ultrathin polymeric films during tensile deformation using atomic force microscopy and digital image correlation techniques," *IEEE Trans. Nanotechnol.*, vol. 6, no. 1, pp. 4–12, Jan. 2007.

[21] H. Wang, J. Zhao, J. Zhao, F. Dong, Z. Pan, and Y. Feng, "Position detection method of linear motor mover based on extended phase correlation algorithm," *IET Sci., Meas. Technol.*, vol. 11, no. 7, pp. 921–928, Oct. 2017.

[22] H. Wang, J. Zhao, J. Zhao, J. Song, Z. Pan, and X. Jiang, "A new rapid-precision position measurement method for a linear motor mover based on a 1-D EPCA," *IEEE Trans. Ind. Electron*, vol. 65, no. 9, pp. 7485–7494, Sep. 2018.

[23] L. Li, D. Pan, and X. Huang, "Analysis and optimization of ironless permanent-magnet linear motor for improving thrust," *IEEE Trans. Plasma Sci.*, vol. 41, no. 5, pp. 1188–1192, May 2013.

[24] M. Debella-Gilo and A. Kääb, "Sub-pixel precision image matching for measuring surface displacements on mass movements using normalized cross-correlation," *Remote Sens. Environ.*, vol. 115, no. 1, pp. 130–142, Jan. 2011.

[25] A. F. Cinar *et al.*, "An autonomous surface discontinuity detection and quantification method by digital image correlation and phase congruency," *Opt. Lasers Eng.*, vol. 96, pp. 94–109, Sep. 2017.

[26] R. Zhang, "Evaluating angular deflections from the digital gradient sensing method with rigid-motion deleted," *Meas. Sci. Technol.*, vol. 27, no. 6, p. 065202, Jun. 2016.

[27] D. Shaokun, Z. Jing, Z. Jiwen, S. Juncai, and W. Hui, "Optimization of the aperiodic fence image for the linear electric motor rotor position measurement," *Chin. J. Sci. Instrum.*, vol. 38, no. 2, pp. 343–350, Feb. 2017.

[28] Y. Su, Q. Zhang, and Z. Gao, "Statistical model for speckle pattern optimization," *Opt. Express*, vol. 25, no. 24, pp. 30259–30275, Nov. 2017.

[29] P. Mazzoleni, F. Matta, E. Zappa, M. A. Sutton, and A. Cigada, "Gaussian pre-filtering for uncertainty minimization in digital image correlation using numerically-designed speckle patterns," *Opt. Lasers Eng.*, vol. 66, pp. 19–33, Mar. 2015.

[30] P. Zhou and K. E. Goodson, "Subpixel displacement and deformation gradient measurement using digital image/speckle correlation," *Opt. Eng.*, vol. 40, no. 8, pp. 1613–1620, Aug. 2001.

[31] P. Lancaster and K. Salkauskas, "Surfaces generated by moving least squares methods," *Math. Comput.*, vol. 37, no. 155, pp. 141–158, 1981.

[32] S.-C. Kang, H.-M. Koh, and J. F. Choo, "An efficient response surface method using moving least squares approximation for structural reliability analysis," *Probabilistic Eng. Mech.*, vol. 25, no. 4, pp. 365–371, Oct. 2010.

[33] B. S. Reddy and B. N. Chatterji, "An FFT-based technique for translation, rotation, and scale-invariant image registration," *IEEE Trans. Image Process.*, vol. 5, no. 8, pp. 1266–1271, Aug. 1996.
[34] L. Zhang *et al.*, "High accuracy digital image correlation powered by GPU-based parallel computing," *Opt. Lasers Eng.*, vol. 69, pp. 7–12, Jun. 2015.

Jing Zhao was born in Huaibei, China. She received the B.S. degree in mechanical engineering from Sichuan University, Chengdu, China, in 2007, and the Ph.D. degree in solid mechanics from the University of Science and Technology of China, Hefei, China, in 2012.

Since 2012, she has been a Lecturer with the School of Electrical Engineering and Automation, Anhui University, Hefei. Her current research interests include optical detection, image processing, and high-precision motion measurement in linear motor system.

Jiwen Zhao was born in Suzhou, China. He received the Ph.D. degree from the University of Science and Technology of China, Hefei, China, in 2005.

Since 2006, he has been with the School of Electrical Engineering and Automation, Anhui University, Hefei, where he is currently a Professor. His current research interests include linear motor optimization design, linear motor control, and photoelectric detection technology.

Hui Wang was born in Fuyang, China. He received the B.S. degree in automation engineering from the Hunan University of Technology, Zhuzhou, China, in 2015. He is currently pursuing the M.E. degree with the School of Electrical Information Engineering, Anhui University, Hefei, China.

His current research interests include optical detection, image processing, and precision motion measurement in linear motor system.

Juncai Song was born in Huainan, China. He received the B.S. and M.E. degrees in electrical engineering from Anhui University, Hefei, China, in 2014 and 2017, respectively, where he is currently pursuing the Ph.D. degree with the School of Electrical Information Engineering.

His current research interests include multiobjective design optimization of permanent magnet synchronous linear motors (PMSLMs), and fault diagnosis and monitoring in PMSLM.

Fei Dong was born in Yuncheng, China. She received the B.S. degree in mechanical engineering and the M.S. degree in mechatronic engineering from Changan University, Xian, China, in 2006 and 2011, respectively.

Since 2011, she has been a Lecturer with the School of Electrical Engineering and Automation, Anhui University, Hefei, China. Her current research interests include the design, analysis, and optimization of permanent magnet synchronous motors.